



ELSEVIER

Contents lists available at ScienceDirect

The Veterinary Journal

journal homepage: www.elsevier.com/locate/tvj

Original article

Ultrasonography, computed tomography and magnetic resonance imaging of the bovine metacarpo/metatarsophalangeal joint

U. Hagag^{a,*}, M.G. Tawfik^b^a Department of Surgery, Anesthesiology and Radiology, Faculty of Veterinary Medicine, Beni-Suef University, Beni-Suef 62511, Egypt^b Department of Anatomy and Embryology, Faculty of Veterinary Medicine, Beni-Suef University, Beni-Suef 62511, Egypt

ARTICLE INFO

Article history:

Accepted 3 January 2018

Keywords:

Bovine
 Computed tomography
 Magnetic resonance imaging
 Metacarpo/metatarsophalangeal joint
 Ultrasonography

ABSTRACT

The aims of the present study were to describe the normal ultrasonographic, magnetic resonance imaging (MRI) and computed tomographic (CT) appearances of the bovine metacarpo/metatarsophalangeal (MCP/MTP) joints and to assess the normal cross-sectional dimensions of the superficial (SDFT) and deep (DDFT) digital flexor tendons. A systematic ultrasound examination was performed on the MCP/MTP joints of 22 healthy cattle and two bovine cadavers, and the cross-sectional dimensions of the SDFT and DDFT were recorded. The cadaveric MCP/MTP joints ($n = 8$) were scanned using a 16-slice multi-detector CT scanner and a 1.5 Tesla MRI scanner, injected with green latex and sectioned into transverse ($n = 4$), sagittal ($n = 2$) and dorsal ($n = 2$) slices. Ultrasonographic, CT and MRI images were correlated with corresponding findings in anatomical dissections for the distal aspects of the third and fourth metacarpal/metatarsal bones, proximal aspects of the proximal phalanges, proximal sesamoid bones, lateral, common and medial digital extensor tendons, SDFT, DDFT, axial and abaxial collateral ligaments, suspensory, palmar/plantar, interdigital intersesamoidean and interdigital phalangosesamoidean ligaments, and collateral, cruciate and short sesamoidean ligaments. The axial and collateral sesamoidean ligaments could not be evaluated by ultrasonography. The articular cartilage, and the short and cruciate sesamoidean ligaments, were not identified in CT images. The cross-sectional dimensions of the SDFT and DDFT differed significantly between the forelimbs and hind limbs ($P < 0.05$); there were no significant differences between the contralateral limbs. The annotated ultrasonographic, CT and MRI images are intended as a normal reference that could be useful for interpretation of clinical disease in the bovine MCP/MTP joint.

© 2018 Elsevier Ltd. All rights reserved.

Introduction

The bovine metacarpo/metatarsophalangeal (MCP/MTP) joint comprises the distal aspects of the third and fourth metacarpal/metatarsal bones, proximal aspects of the corresponding proximal phalanges and two pairs of proximal sesamoid bones (Budras et al., 2011). The joint is reinforced by multiple ligaments and tendons. Ligaments include the axial and abaxial collateral ligaments, suspensory ligament, palmar/plantar ligaments, interdigital intersesamoidean ligaments, collateral sesamoidean ligaments, cruciate sesamoidean ligaments, interdigital phalangosesamoidean ligament and the short sesamoidean ligaments. The MCP/MTP tendons include the lateral digital extensor tendon,

medial digital extensor tendon, common digital extensor tendon, superficial digital flexor tendon (SDFT) and the deep digital flexor tendon (DDFT). The MCP/MTP joint has a smaller dorsal recess compared to the larger palmar/plantar recess (Dyce et al., 2010).

Lameness is a significant worldwide problem that has substantial welfare implications and an important economic impact on dairy farms (Solano et al., 2015). The MCP/MTP joint is an important source of lameness (Starke et al., 2006), accounting for 27% of monoarthritis in adult cattle (Meier, 1997). A thorough physical examination is usually performed to diagnose lameness originating from the MCP/MTP joint (Rohde et al., 2000), but can be challenging in cattle with swollen joints (Starke et al., 2007). In such instances, diagnostic imaging modalities, including radiography, ultrasonography, computed tomography (CT) and magnetic resonance imaging (MRI), may improve the likelihood of a definitive diagnosis, with potential benefits for prognosis and treatment in affected cattle (Kofler et al., 2014).

* Corresponding author.

E-mail address: usama.hagag@vet.bsu.edu.eg (U. Hagag).

Radiography and ultrasonography are used for most diagnostic medical imaging in bovine practice (Kofler et al., 2014); ultrasonography is superior for diagnosis of soft tissue disorders, particularly tendonitis and tenosynovitis (Kofler, 2006). Ultrasonographic assessment of tendon injury depends mainly on changes in size and echogenicity. A thorough knowledge of the normal echogenic appearance of the structures examined is important in order to recognise features of injury, to avoid misinterpretation and to prevent false positive diagnoses. The normal ultrasonographic characteristics of the MCP/MTP synovial structures and pouches have been described in cattle (Kofler and Edinger, 1995). The normal cross-sectional dimensions of the SDFT and DDFT have been reported in Nellore and Girolando calves (Gonçalves et al., 2014). However, the normal echogenic features and cross-sectional dimensions of the SDFT and DDFT in adult cattle have not been reported.

CT and MRI have proven valuable for diagnosis of a wide range of musculoskeletal disorders in veterinary practice (Bienert and Stadler, 2006). The main advantages of CT and MRI, compared to radiography and ultrasonography, are three dimensional imaging and concurrent visualisation of bone and soft tissue structures without superimposition (Kraft and Gavin, 2001). The benefits of CT include better bone contrast and a shorter time for examination, while MRI is superior for evaluation of soft tissues and subchondral bone changes (Tucker and Sande, 2001). Concurrently, there is growing interest in the use of CT and MRI in bovine orthopaedics (Nuss et al., 2011) and clinical reports involving CT and MRI have been published (Van Biervliet et al., 2004; Lubbers et al., 2007; Raji et al., 2008, 2009; Becker et al., 2011; Ehlert et al., 2011; Lee et al., 2011; Tsuka et al., 2015; Hagag et al., 2016).

An understanding and knowledge of the descriptive, topographical and cross-sectional features of anatomical structures is necessary for successful diagnostic image interpretation (Latorre and Rodríguez, 2007). The aims of the present study were: (1) to describe the normal ultrasonography, CT and MRI appearances of the bovine MCP/MTP joint; (2) to correlate ultrasonographic, CT and MRI images of the MCP/MTP joint with their corresponding anatomical sections; and (3) to provide the ultrasonographic cross-sectional dimensions of the SDFT and DDFT in adult cattle and assess symmetry between limbs.

Materials and methods

Animals

Ultrasound examination was carried out on the MCP/MTP joints ($n=88$) of 22 adult healthy non-pregnant Holstein-Friesian cows, with a mean age \pm standard deviation (SD) of 7.5 ± 3.3 years and a mean weight \pm SD of 498.8 ± 65.0 kg. Animals were confirmed to be free of lameness via locomotion scoring (Sprecher et al., 1997). Ultrasonographic, CT and MRI examinations were carried out on the MCP/MTP joints ($n=8$) of two fresh cattle cadavers euthanased for reasons unrelated to musculoskeletal disorders. Examinations were carried out within 6 h after euthanasia. The study was approved by the Institutional Animal Care and Use Committee of Beni-Suef University, Egypt (IACUC001/2017; date of approval 3 January 2017).

Ultrasonographic study

Animals were restrained in a chute and the limb to be examined was secured. The MCP/MTP region was clipped, washed with warm water, saturated with 70% alcohol and contact gel was applied. A B-mode ultrasound examination (Eickemeyer Magic 5000 Digital ultrasound machine, Eickemeyer Veterinary Equipment) was carried out using 5–10 MHz linear transducer with a 4–5 cm depth of penetration. The measurement accuracy of the machine was 0.4 mm as per the manufacturers' guidelines.

Ultrasound examination was first performed on standing cows with the examined limb in weight-bearing position. The MCP/MTP joint was imaged from proximal to distal in both transverse and longitudinal planes using dorsal, palmar/plantar, medial and lateral approaches. On the palmar/plantar aspect of the MCP/MTP joint at the apices of the proximal sesamoid bones, two defined distances were measured in the transverse plane via electronic callipers to assess the width (maximum lateromedial borders) and thickness (dorsopalmar/plantar limits) of the DDFT and the thickness (dorsopalmar/plantar limits) of the SDFT (Fig. 6). Measurements were carried out with cows bearing full weight on all limbs. Since the dorsal soft tissues of the MCP/MTP joint were relaxed in the weight-bearing position, complementary longitudinal and transverse imaging of these structures was also performed on the flexed joint with the limb in a non-weight bearing position.

Magnetic resonance imaging study

Limbs were extended and placed with the lateral aspect as the dependent portion and long axis of the limb parallel to the examination table. T1-weighted gradient echo (GRE) images ($TR=1900$ ms; $TE=2.74$ ms; slice thickness = 3 mm) were obtained in sagittal, dorsal and transverse planes using a 1.5 Tesla magnet (Philips Ingenia 1.5 T, Philips GmbH).

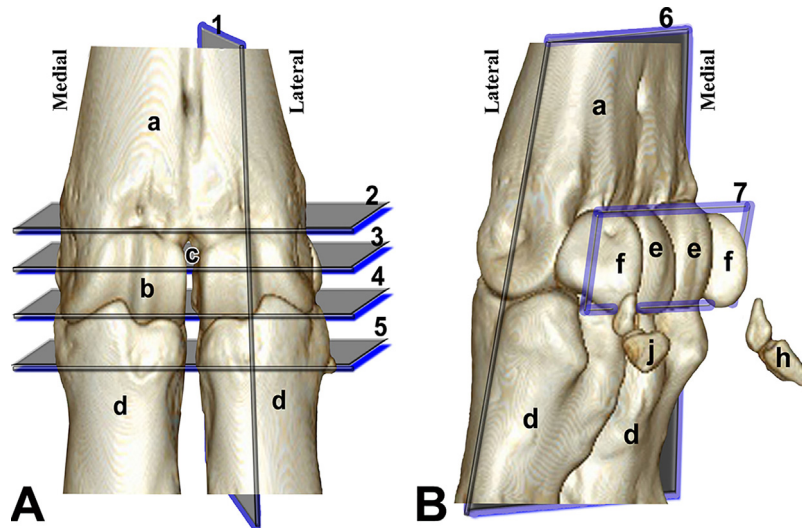


Fig. 1. Three dimensional reconstructed views of the normal bovine metacarpus/metatarsophalangeal joint. Numbered sections indicate the approximate levels of each anatomical slice and the corresponding computed tomography (CT) and magnetic resonance imaging (MRI) depictions. (A) Dorsal view showing the selected sagittal (1) and transverse (2–5) sections. (B) Palmar/plantarolateral view showing the selected planes for the dorsal (6–7) sections. a, metacarpus/metatarsus; b, sagittal ridge; c, intercapitral notch; d, proximal phalanx; e, axial sesamoid bones; f, abaxial sesamoid bones; j, rudimentary digit V; h, rudimentary digit II.

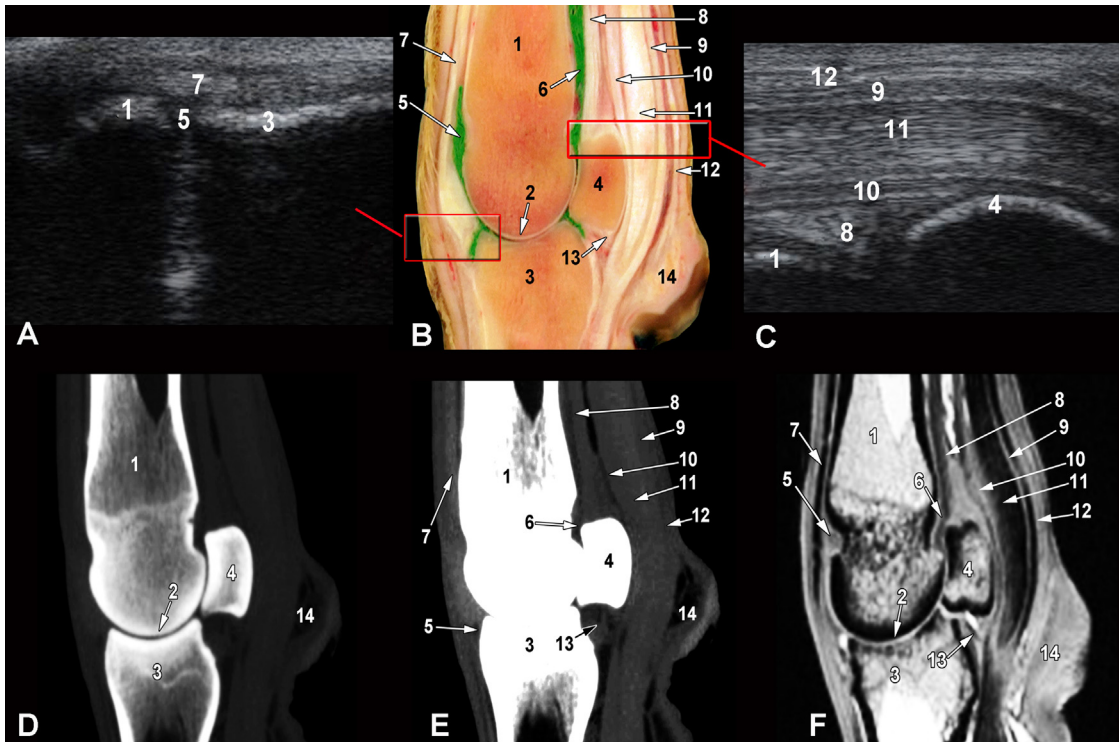


Fig. 2. Parasagittal/longitudinal images of the metacarpophalangeal joint. (A) Longitudinal ultrasound (US) image acquired from a dorsolateral approach. (B) Parasagittal anatomical section. (C) Longitudinal US image acquired from a palmar approach. (D) Bone window computed tomography (CT) image in a bone kernel. (E) CT image in a soft tissue kernel. (F) Magnetic resonance imaging (MRI) representation at the level of the sagittal ridge of the fourth metacarpus bone (level 1 as indicated in Fig. 1). 1, Fourth metacarpal bone; 2, subcondylar bone; 3, proximal phalanx; 4, proximal sesamoid bone; 5, dorsal synovial pouch; 6, palmar synovial pouch; 7, lateral digital extensor tendon; 8, suspensory ligament; 9, superficial digital flexor tendon (SDFT); 10, manica flexoria; 11, deep digital flexor tendon (DDFT); 12, annular ligament; 13, interdigital phalangesesamoidean ligament; 14, dew claw.

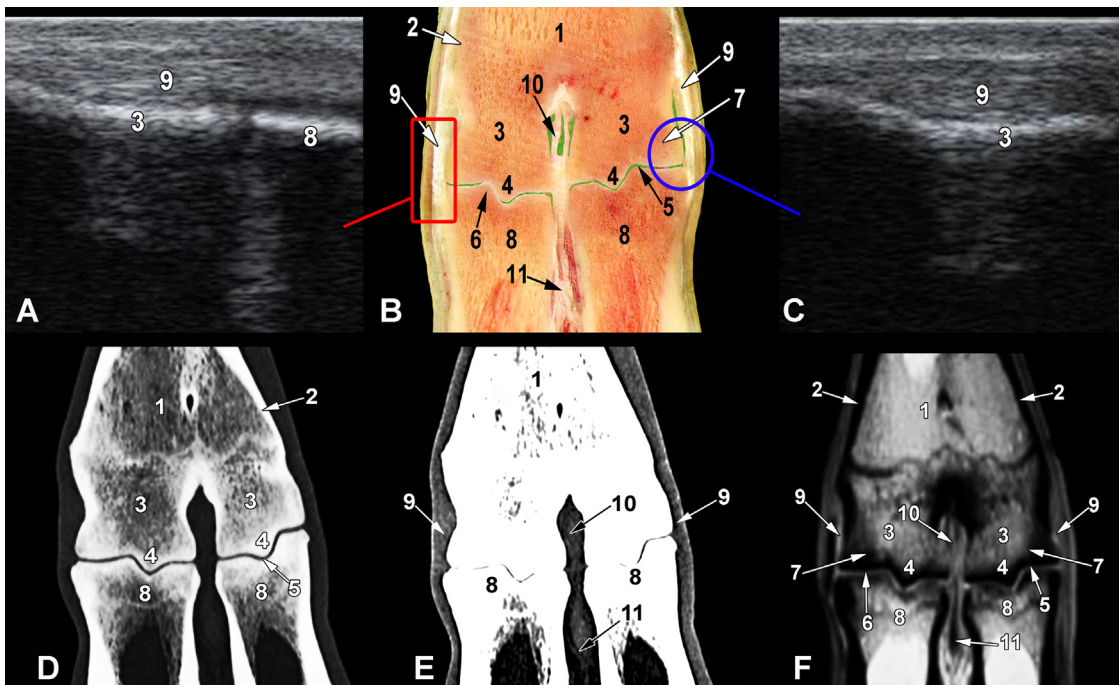


Fig. 3. Metatarsophalangeal joint. (A) Longitudinal ultrasound (US) image acquired from a lateral approach. (B) Parasagittal anatomical section. (C) Transverse US image acquired from a lateral approach. (D) Bone window computed tomography (CT) image in a bone kernel. (E) CT image in a soft tissue kernel. (F) Magnetic resonance imaging (MRI) representation acquired at the level of collateral ligament attachment (level 6 as indicated in Fig. 1). 1, Metatarsus; 2, cortical bone; 3, cancellous bone; 4, sagittal ridge; 5, metatarsophalangeal articulation; 6, articular cartilage; 7, subchondral bone; 8, proximal phalanx; 9, abaxial collateral ligaments; 10, axial collateral ligaments; 11, proximal interdigital ligament.

Computed tomography study

CT scanning was conducted using a helical CT scanner (Philips Mx8000 IDT 16 CT scanner; Philips GmbH) and limbs were positioned as in the MRI study. A scout image (120 kV and 50 mA) was obtained to ensure symmetry in positioning and inclusion of the entire region of interest. The acquisition settings were 120 kV and 150 mA, collimation of 0.75 mm, increment of 0.6 mm, rotation time of 1 s, pitch of 0.85, field of view of 20 cm, slice thickness of 1 mm, and matrix size of 512. The transverse CT images were reformatted into sagittal and dorsal slices, then images from all limbs were reviewed in 'bone window' (window width=3000, window level=600) and 'soft tissue window' (window width=300, window level=120), and the attenuation (density) of each structure was recorded.

Anatomical study

At the conclusion of MRI and CT scans, the MCP/MTP joints (*n*=8) were injected with green latex. The needle (G18, 1.2 mm × 40 mm) was introduced abaxial to the tendinous portions of the common digital extensor muscle into the dorsal pouch. Limbs were frozen at -20 °C, and then sectioned into dorsal (forelimb: *n*=1; hind limb: *n*=1), sagittal (forelimb: *n*=1; hind limb: *n*=1) and transverse (forelimb: *n*=2; hind limb: *n*=2) cryosections at approximately 5–10 mm thickness by means of an electric band saw. All anatomical sections were inspected; structures were identified and correlated with their corresponding ultrasound, MRI and CT images on the basis of shape, size, location and tissue density characteristics.

Comparison of imaging findings with anatomical sections

The ultrasound, MRI and CT images, as well as anatomical sections, of the MCP joint were compared to their corresponding images of the MTP joint on the basis of shape, size, location and tissue density characteristics. All measurements were performed by a single operator and all images (ultrasonography, CT and MRI) were reviewed by the both authors. For interpretation of different structures of the MCP/MTP joint, seven CT and MRI images were selected as being representative for the main anatomical structures (Fig. 1) in conjunction with their corresponding

anatomical sections, one in a sagittal plane (Fig. 2), two in a dorsal plane (Figs. 3 and 4) and four in a transverse plane (Figs. 5–8). Representative ultrasonograms were correlated with their corresponding anatomical, CT and MRI images (Figs. 2, 3 and 6).

Statistical analysis

Data were analysed using SPSS for Windows version 16 (IBM). Results are given as means ± SDs (Table 1). The differences between the cross-sectional dimensions of the axial and abaxial SDFT and DDDFT of the same limb and the contralateral limb, and between the forelimbs and hind limbs, were determined using an independent sample *t* test. *P*<0.05 was considered to be significant.

Results

Comparison of anatomical sections with ultrasound, CT and MRI images allowed a precise analysis and description of the normal ultrasonographic, CT and MRI appearance of the bovine MCP/MTP joint. No morphological or topographical variations were detected between the left and right contralateral limbs, or between the MCP and MTP joints.

Ultrasonography

The lateral, common and medial digital extensor tendons were identified as ovoid structures over the dorsal aspect of the MCP/MTP joint (Fig. 6). The lateral digital extensor tendon was larger than the medial tendon, while the common digital extensor tendon was the largest. They had less echogenic and coarser appearances than the flexor tendons (Fig. 2). Bone surfaces of the metacarpal/

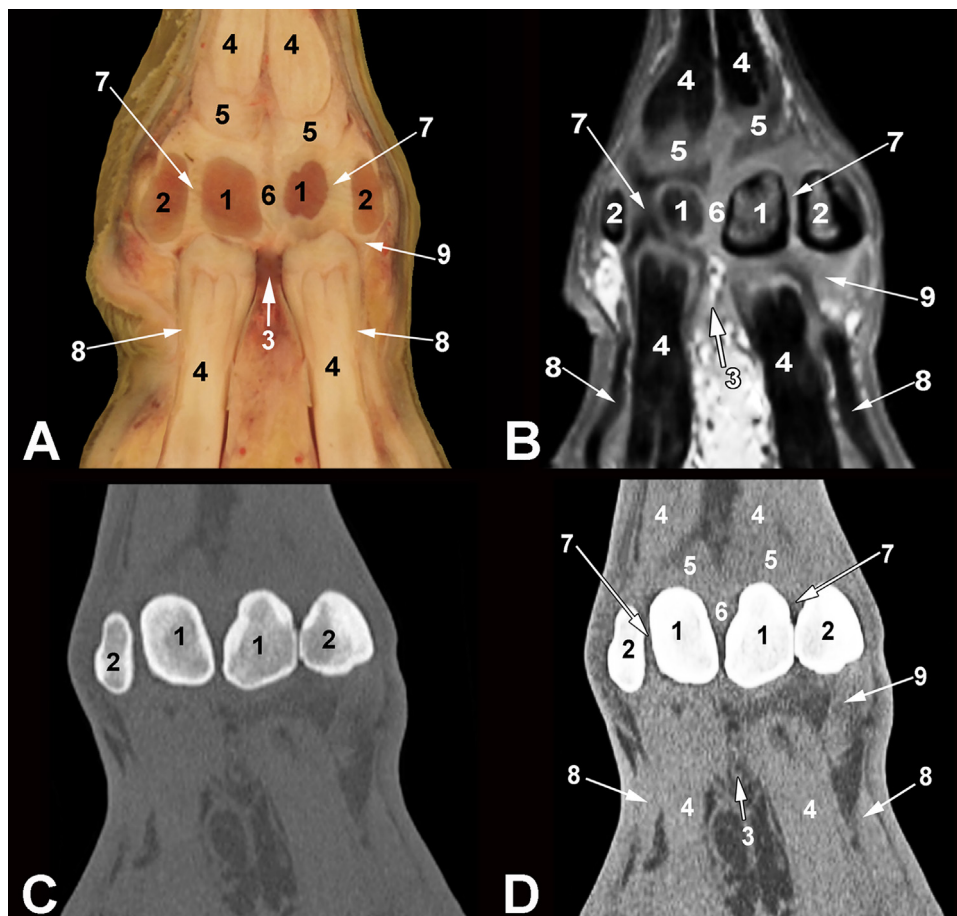


Fig. 4. Metacarpophalangeal joint at the level of the proximal sesamoid bones (level 7 as indicated in Fig. 1). (A) Dorsal anatomical section. (B) Magnetic resonance imaging (MRI). (C) Bone window computed tomography (CT) image in a bone kernel. (D) CT image in a soft tissue kernel. 1, axial sesamoid bones; 2, abaxial sesamoid bones; 3, proximal interdigital ligament; 4, deep digital flexor tendon (DDFT); 5, manica flexoria; 6, interdigital intersesamoidean ligament; 7, palmar ligaments; 8, superficial digital flexor tendon (SDFT); 9, collateral sesamoidean ligament.

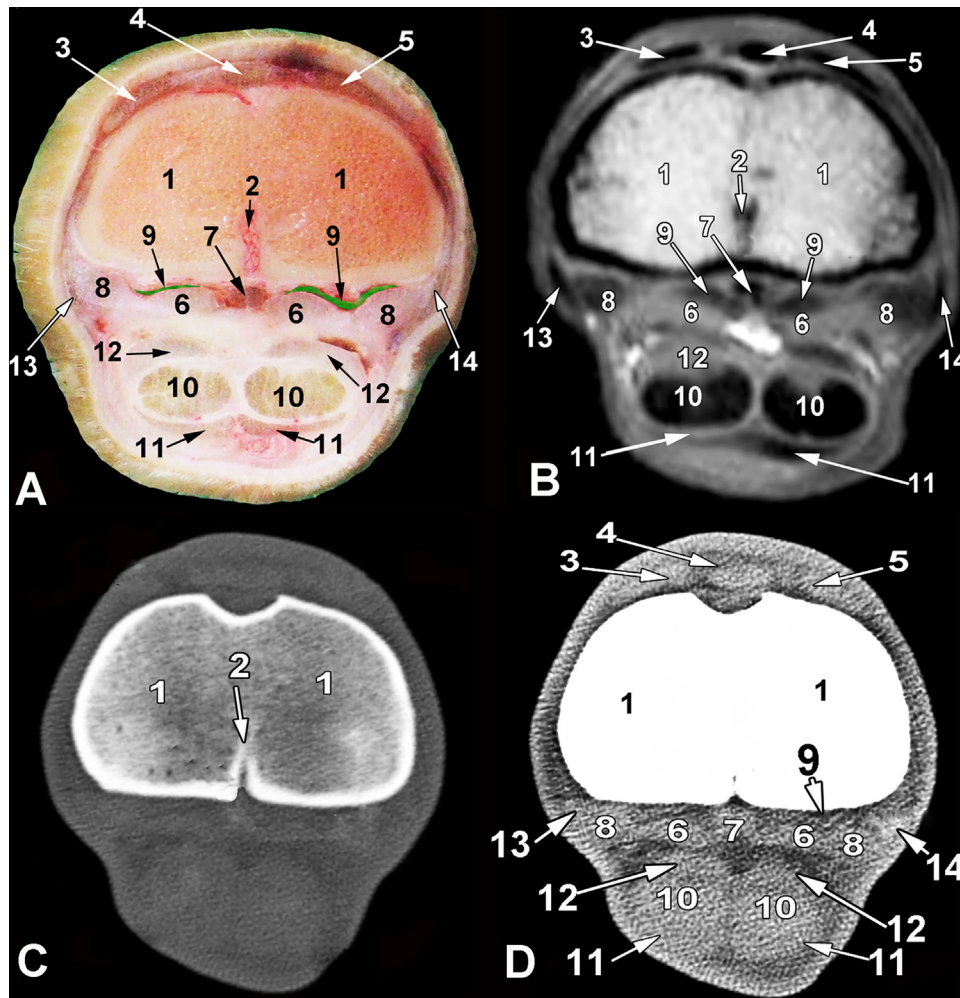


Fig. 5. Metacarpophalangeal joint at the level of the distal third of the metacarpus (level 2 as indicated in Fig. 1). (A) Transverse anatomical section. (B) Magnetic resonance imaging (MRI). (C) Bone window computed tomography (CT) image in a bone kernel. (D) CT image in a soft tissue kernel. 1, Metacarpus; 2, intercapital notch; 3, lateral digital extensor tendon; 4, common digital extensor tendon; 5, medial digital extensor tendon; 6, collateral fibres of suspensory ligament middle limb; 7, interdigital fibres of suspensory ligament middle limb; 8, deep fibres of collateral suspensory ligament; 9, palmar synovial pouch; 10, deep digital flexor tendon (DDFT); 11, superficial digital flexor tendon (SDFT); 12, manica flexoria; 13, suspensory ligament lateral abaxial part; 14, suspensory ligament medial abaxial part.

metatarsal condyles and proximal phalanges had regular, smooth, hyperechoic contours. In the weight-bearing position, the dorsal aspects of the subchondral bone of the metacarpal/metatarsal condyles, the sagittal ridge and the proximodorsal surface of the proximal phalanges appeared as hyperechogenic lines. Most of the metacarpal/metatarsal articular surface was evaluated during joint flexion, while the articular surface of the proximal phalanges could not be assessed. The articular cartilage was recognised as a hypoechoic smooth band that was thickest over the sagittal ridge and thinner over the condyles. The joint capsule was difficult to discern from the overlying soft tissue structures. The dorsal joint pouch was depicted in the longitudinal plane as an anechoic area (articular cartilage) between the hyperechoic bone surfaces that increased during joint flexion (Fig. 2). No synovial fluid was visualised; thus, joint pouches could not be delineated.

The abaxial collateral ligaments were evaluated in both longitudinal and transverse planes from their origin on the metacarpal/metatarsal condylar fossa until their insertion onto the contralateral proximal phalanx. They had a uniformly distributed, coarse, echogenic pattern overlying the hyperechoic bone surface (Fig. 3). The axial collateral ligaments could not be evaluated.

The SDFT, DDFT, branches of the suspensory ligament (middle interosseous muscle) and the palmar/plantar annular ligament were clearly distinguished and had a homogeneous echogenic appearance. The DDFT was more echogenic than the SDFT, and the suspensory ligament was less echogenic than the SDFT and DDFT (Figs. 2 and 6). In the transverse plane, the SDFT was crescentic in shape, with sharp edges forming a ring (manica flexoria) around the DDFT (Fig. 6). The DDFT was ovoid, with smooth and well defined borders. In the longitudinal plane, the SDFT and DDFT had a regular continuous linear pattern (Fig. 2). The apices of the proximal sesamoid bones were recognised as hyperechogenic lines covered palmar/plantarly by the flexor tendons. The body and base of the proximal sesamoid bones, as well as the palmar/plantar interdigital intersesamoidean, collateral sesamoidean, interdigital phalangosamoidean, short sesamoidean and cruciate sesamoidean ligaments, could not be evaluated.

The average measurements of the SDFT and DDFT are shown in Table 1. The palmar/plantar joint pouch could not be distinguished. The margins of the digital flexor tendon synovial sheaths were only recognised as hyperechoic lines separating tendons without fluid accumulation. No significant differences were found between the measurements of the SDFT and DDFT in the same or contralateral

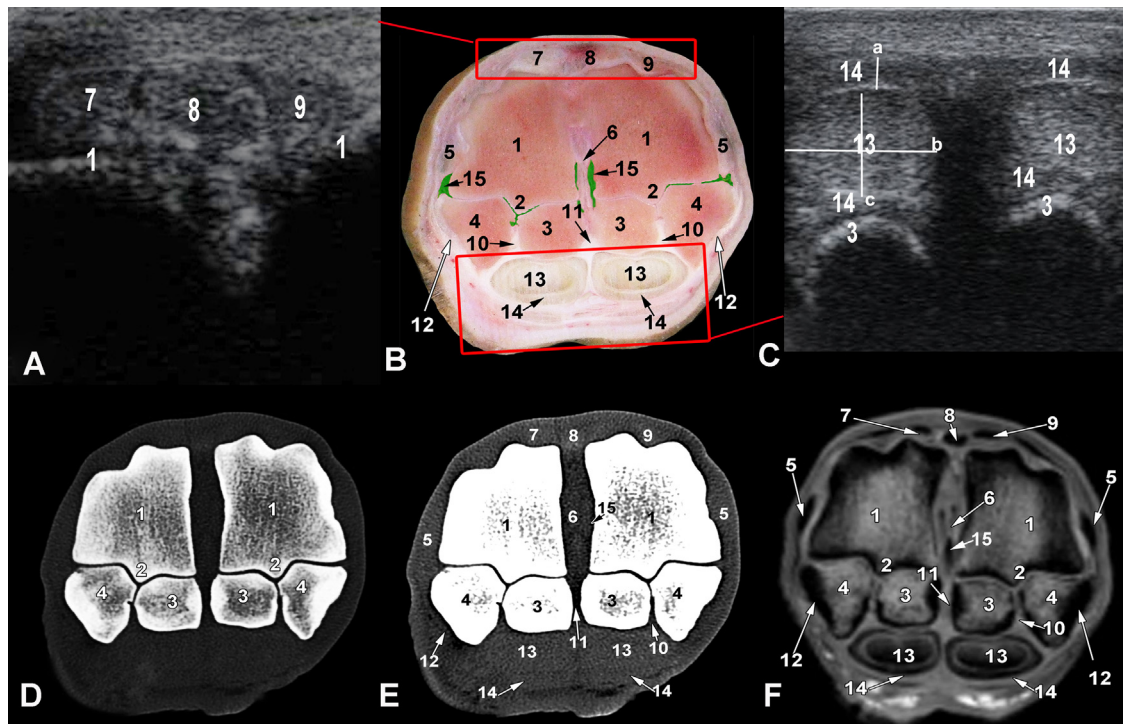


Fig. 6. Transverse images of the metatarsophalangeal joint. (A) Transverse ultrasound (US) image acquired from a dorsal approach. (B) Transverse anatomical section. (C) Transverse ultrasound US image acquired from a plantar approach. (D) Bone window computed tomography (CT) image in a bone kernel. (E) CT image in a soft tissue kernel. (F) Magnetic resonance imaging (MRI) representation at the level of the middle third of the proximal sesamoid bones (level 3 as indicated in Fig. 1). a, Superficial digital flexor tendon (SDFT) thickness; b, deep digital flexor tendon (DDFT) width; c, DDFT thickness. 1, Metatarsus; 2, sagittal ridge; 3, axial sesamoid bones; 4, abaxial sesamoid bones; 5, abaxial collateral ligaments; 6, axial collateral ligaments; 7, lateral digital extensor tendon; 8, common digital extensor tendons; 9, medial digital extensor tendon; 10, plantar ligaments; 11, interdigital intersesamoidean ligament; 12, collateral sesamoidean ligament; 13, DDFT; 14, SDFT; 15, plantarsynovial pouch.

limbs; however, statistically significant differences were detected between the forelimbs and hind limbs ($P < 0.05$).

Magnetic resonance imaging

The MRI appearance of the normal MCP/MTP joint is illustrated in Figs. 2–8. Sagittal images (Fig. 2) showed excellent differentiation of synovial fluid, synovial membrane, articular cartilage and subchondral bone, while in dorsal images (Figs. 3 and 4) there was good definition of collateral ligaments and collateral sesamoidean ligaments. In transverse images (Figs. 5–8), there was a good definition of bone, especially the proximal sesamoid bones. These sections provided considerable information about the extent of synovial pouches and their relationships with collateral ligaments and joint capsule.

The articular cartilage was clearly defined from adjacent bone and appeared as a layer of homogeneous high signal intensity with a smooth osteochondral junction. The subchondral bone plate was evident as an area of homogeneous low signal intensity, and was easily defined from articular cartilage on one border and cancellous bone on the other. Cortical bone had homogeneous low signal intensity, with a regular and clearly defined cortico-cancellous junction. Cancellous bone had heterogeneous signal intensity and a well-defined trabecular pattern.

Soft tissue structures identified by MRI, including the lateral, common and medial digital extensor tendons, the SDFT and the DDFT, had homogeneous low signal intensity. Ligaments, including the axial and abaxial collateral ligaments, annular ligament, suspensory ligament, palmar/plantar ligaments, interdigital intersesamoidean ligaments, collateral sesamoidean ligaments and interdigital phalangesesamoidean ligament, had heterogeneous intermediate signal intensity. The cruciate and short sesamoidean ligaments could be localised, but could not at all times be identified

clearly. The digital flexor tendon sheath was recognised as a thin structure of low signal intensity. Tendon margins were clearly defined by the surrounding fascia, which had intermediate signal intensity. The margins of the joint capsule were clearly delineated and appeared as a fine line of intermediate signal intensity.

Computed tomography

In the 'bone window', the diaphysis, condyles and sagittal ridges of the metacarpus/metatarsus, axial and abaxial proximal sesamoid bones, and proximal phalanges, had smooth margins and could be recognised on the transverse, sagittal and dorsal CT images. All images had excellent delineation between the cortex and medulla of bones, with clear depiction of the trabecular pattern. In the 'soft tissue window', bones appeared hyperdense and soft tissues were represented by variable densities. The lateral, common and medial extensor tendons, and the SDFT and DDFT, were best evaluated on transverse CT images as hyperdense structures compared with the surrounding hypodense connective tissue and joint capsule. Ligaments, including the axial and abaxial collateral ligaments, annular ligament, suspensory ligament, palmar/plantar ligaments, interdigital intersesamoidean ligaments, collateral sesamoidean ligaments and interdigital phalangesesamoidean ligament, were well defined, clearly outlined and were best evaluated on the transverse and dorsal CT images (Figs. 2–8). The cruciate and short sesamoidean ligaments could not be identified.

Discussion

The present study provides detailed ultrasonographic, CT and MRI reference images of the clinically relevant structures of the bovine MCP/MTP joint, together with their corresponding

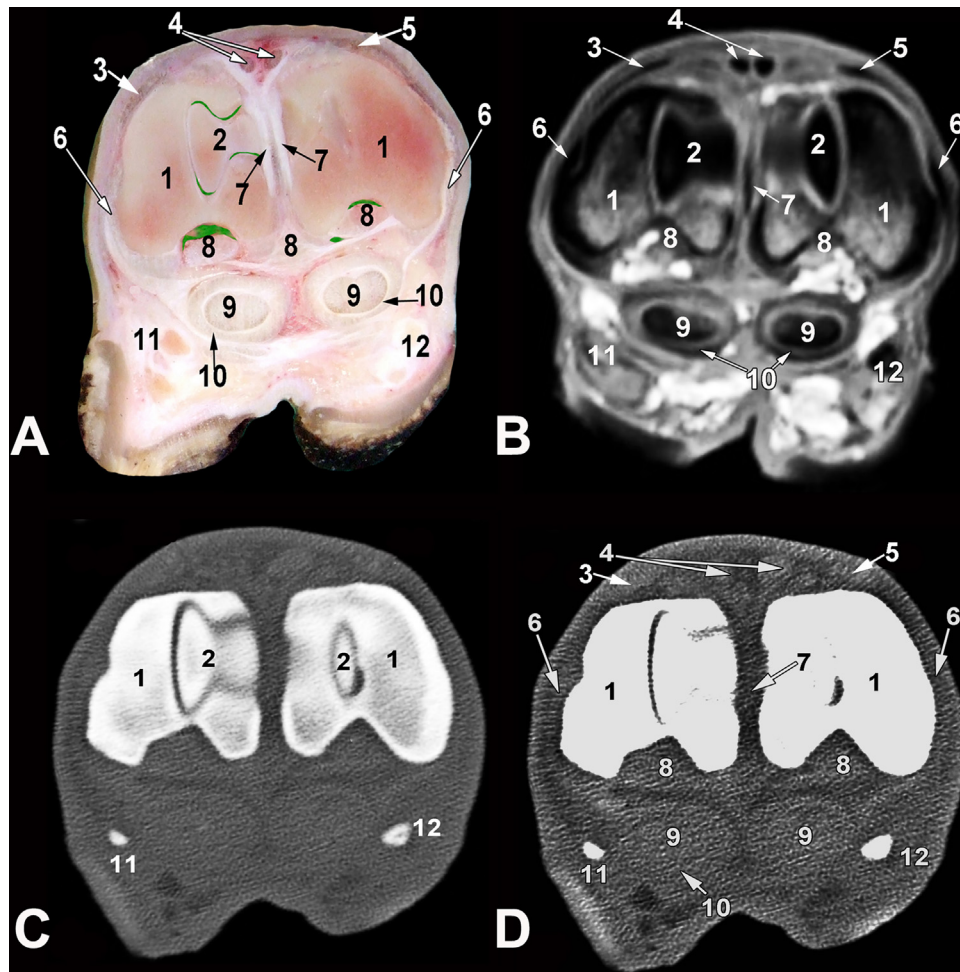


Fig. 7. Metacarpophalangeal joint at the level of the joint space (level 4 as indicated in Fig. 1). (A) Transverse anatomical section. (B) Magnetic resonance imaging (MRI) representation. (C) Bone window computed tomography (CT) image in a bone kernel. (D) CT image in a soft tissue kernel. 1, proximal phalanges (III and IV); 2, sagittal ridge of the metacarpus; 3, lateral digital extensor tendon; 4, common digital extensor tendons; 5, medial digital extensor tendon; 6, abaxial collateral ligaments; 7, axial collateral ligaments; 8, suspensory ligament; 9, deep digital flexor tendon (DDFT); 10, superficial digital flexor tendon (SDFT); 11, rudimentary digit V; 12, rudimentary digit II.

anatomical sections. These images should augment the clinical use of multiple imaging modalities in diagnosing bovine MCP/MTP joint disorders.

In this study, a stand-off pad was not used, since it was cumbersome and decreased the clarity of the image. Using a high resolution linear transducer with superior near-field resolution and a broad superficial field of view was helpful in evaluating superficial structures. This is consistent with previous reports of ultrasonography in cattle (Kofler, 1996; Heppelmann et al., 2009) and horses (Pickersgill et al., 2001; Vanderperren et al., 2012).

Owing to the division of the SDFT and DDFT into medial and lateral subdivisions at the level of the MCP/MTP joint, as well as the size of transducer, visualisation of the SDFT borders was not possible. To visualise these structures consistently, each of the medial and lateral flexor tendons was assessed individually.

A thorough, systematic ultrasonographic examination of the MCP/MTP joint was achieved. The joint was divided into four areas (dorsal, palmar/plantar, medial and lateral), and each area was investigated from proximal to distal in both longitudinal and transverse planes. A similar approach has been described in the horse (Denoux et al., 1996; Seignour et al., 2012); however, ultrasonographic examination of the MCP/MTP joint in cattle showed some limitations. Due to the anatomical differences between cattle and horses, the axial collateral ligaments could not

be evaluated owing to their anatomical position. Furthermore, the palmar/plantar, interdigital intersesamoidean, collateral sesamoidean, interdigital phalangosesamoidean, short sesamoidean and cruciate sesamoidean ligaments could not be examined, since they were masked by the dew claws; these are absent in horses.

Septic inflammation of the digital flexor tendons is a common cause of lameness in cattle (Kofler, 1996). Ultrasonography is the technique of choice to identify tendon and other soft tissue disorders (Kofler and Edinger, 1995). Ultrasonographic assessment of tendon injury could be judged by comparison with other structures visible in the ultrasonogram, comparison with the contralateral limb or measurement of tendon cross-sectional dimensions (Genovese et al., 1986). Provision of reference data provides guidelines for veterinary clinicians to evaluate the SDFT and DDFT tendons, where alteration in these values would indicate tendon pathology.

In the present study, the normal ultrasonographic cross-sectional dimensions of the DDFT and SDFT were determined. Measurements were obtained at the apices of the proximal sesamoid bones, where there were no skin folds that could impede the contact of the transducer with the skin surface (Kofler, 1996). Examinations were performed by the same person according to a set protocol to improve the reliability of sonography and reduce operator variability. The measurements were carried out with the

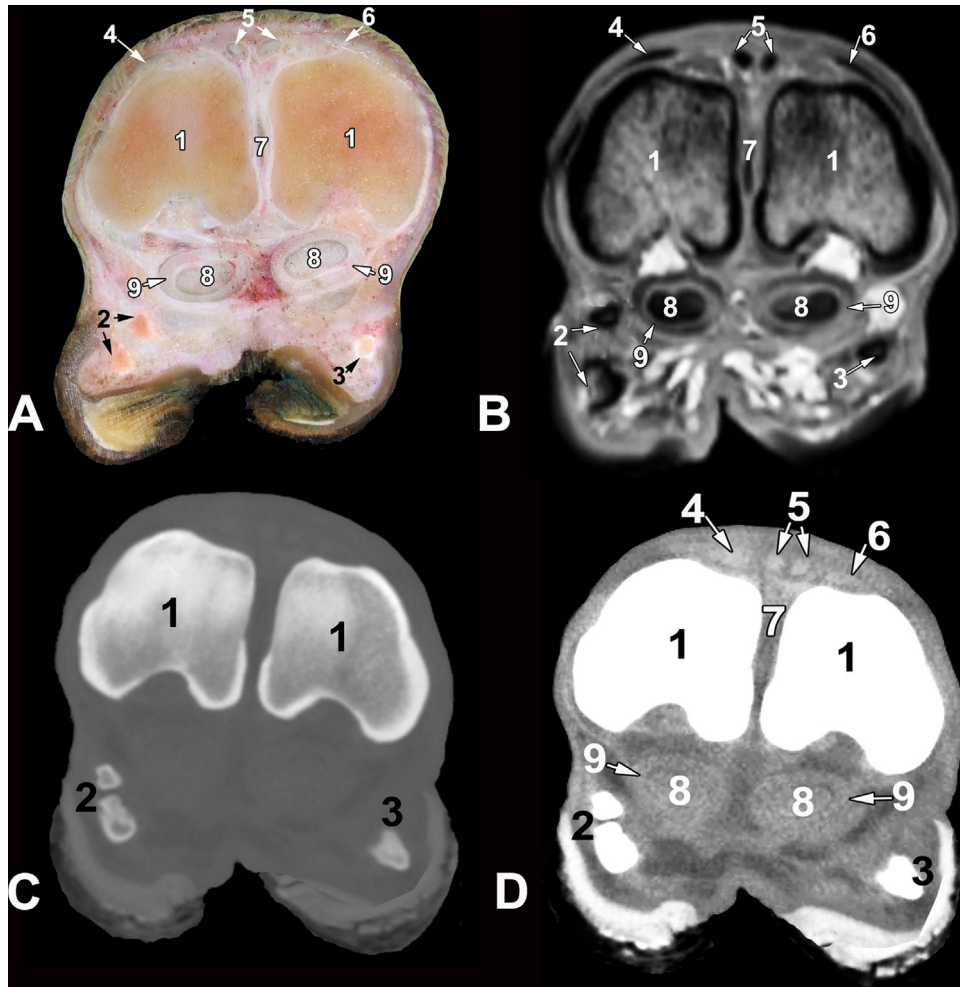


Fig. 8. Metatarsophalangeal joint at the level of proximal phalanges (level 4 as indicated in Fig. 1). (A) Transverse anatomical section. (B) Magnetic resonance imaging (MRI) representation. (C) Bone window computed tomography (CT) image in a bone kernel. (D). CT image in a soft tissue kernel. 1. Proximal phalanx; 2, rudimentary digit V; 3, rudimentary digit II; 4, lateral digital extensor tendon; 5, common digital extensor tendons; 6, medial digital extensor tendon; 7, proximal interdigital ligament; 8, deep digital flexor tendon (DDFT); 9, superficial digital flexor tendon (SDFT).

Table 1

Means ± standard deviations (SD) of the superficial (SDFT) and deep (DDFT) digital flexor tendon cross-sectional dimensions (cm).

		Forelimb				Hind limb			
		Right		Left		Right		Left	
		Lateral	Medial	Lateral	Medial	Lateral	Medial	Lateral	Medial
SDFT	Thickness	0.35 ± 0.04	0.31 ± 0.07	0.34 ± 0.05	0.31 ± 0.02	0.26 ± 0.05	0.28 ± 0.05	0.25 ± 0.05	0.29 ± 0.05
DDFT	Thickness	0.89 ± 0.15	0.91 ± 0.11	0.84 ± 0.11	0.93 ± 0.18	0.82 ± 0.19	0.84 ± 0.15	0.83 ± 0.11	0.81 ± 0.12
	Width	1.82 ± 0.07	1.85 ± 0.21	1.81 ± 0.15	1.84 ± 0.17	1.78 ± 0.23	1.80 ± 0.22	1.75 ± 0.18	1.77 ± 0.24

limb in a weight-bearing position, since tension applied on tendons would affect the ultrasonographic measurements. In the non-weight bearing limb, tendons would be relaxed, potentially resulting in misinterpretation of ultrasonographic images (Boehart et al., 2010). The lateromedial width of the SDFT was not considered in this study, since the SDFT at the level of the MCP/MTP joint encircles the DDFT, forming the manica flexoria, and the selection of corresponding sonographic reference points was difficult.

No significant differences were found between the mean values of the cross-sectional dimensions of the axial and abaxial SDFT and DDFT of the same or contralateral limbs. These findings shared some similarity to those described in horse (Smith et al., 1994). A

significant difference was detected between the forelimbs and hind limbs; this might be due to the increased load on the hind limbs (Chapinal et al., 2009). No other differences in anatomical, ultrasound, CT or MRI features between the MCP and MTP joints were identified, although no formal comparison of measurements, other than for the SDFT and DDFT, was made between the MCP and MTP joints.

The present study demonstrates that CT and MRI are useful techniques for imaging the bovine MCP/MTP joint. A T1-weighted GRE MRI pulse sequence was used to generate a high level of anatomical detail, with minimal thickness and contiguous slices, obtained at a high acquisition speed; these parameters would be appropriate for practical clinical scanning (Smith et al., 2011).

CT and MRI enabled visualisation of the bovine MCP/MTP joint in three planes and multiple slices, allowing the veterinary clinician to evaluate joint structures at numerous angles. The use of latex injected synovial pouches permitted an accurate and detailed description of anatomical features, and provided some clinical reference standards for the shape and position of the normal anatomical structures. All major soft tissue structures were clearly outlined on both MRI and CT images. Similar findings have been reported in the horse (Dyson and Murray, 2007). However, in this study, the short and cruciate sesamoidean ligaments, as well as the articular cartilage, could not be assessed using CT in cattle; the latter could be visualised either by MRI or CT arthrography (Vanderperren et al., 2008).

In the present study, MRI permitted evaluation of the articular cartilage of the proximal phalanges; these could not be assessed using ultrasonography. Similar findings have been reported in the horse (Dyson and Murray, 2007). Although MRI has been reported to be a good imaging modality for evaluation of articular cartilage, accurate MRI evaluation of degenerative and traumatic cartilage lesions in the distal limb remains difficult (O'Brien et al., 2011). Imaging difficulties arise because the cartilage frequently is too thin for the spatial resolution of clinical MRI. In addition, the articular surfaces of the distal limb joints are markedly curved. Both factors promote partial volume-averaging across image slices, resulting in blurring of cartilage margins (Cohen et al., 1999).

In cattle, septic arthritis is a common cause of MCP/MTP lameness (Meier, 1997; Starke et al., 2006), resulting from punctures/trauma or spread of infection from neighbouring tissues. Diagnosis of septic arthritis relies on suggestive clinical findings (lameness, pain, effusion and swelling), and a judicious choice of radiography and/or ultrasonography (Heppelmann et al., 2009). Radiography will reveal soft tissue swelling, but does not permit evaluation of synovial effusion or the extent of infection (Kofler, 1996).

Ultrasonography can be used to detect the early stages of synovial effusion based on synovial pouch distension. Ultrasonography is a safe, non-invasive modality, providing accurate real-time diagnostic information relating to soft tissues, cartilage and the subchondral bone of bovine joints (Kofler et al., 2014). However, ultrasonography is highly operator and equipment dependent, cannot be used to evaluate structures deep to the bone surface and has a restricted field of view (Relave et al., 2009). Therefore, additional modalities, such as CT and MRI, are sometimes required to arrive at a conclusive diagnosis.

CT and MRI are becoming more readily available and commonly used for diagnosis of bovine orthopaedic disorders (Lee et al., 2011). CT provides excellent detail of osseous structures and can detect bone changes before they are clinically or radiographically apparent (Young et al., 2007). Moreover, soft tissues could be evaluated via CT (Bienert and Stadler, 2006; Vanderperren et al., 2008). MRI affords a high soft tissue contrast, provides anatomical and physiological information in multiple planes, does not use ionising radiation, and can simultaneously provide images of bone and soft tissues with a better soft tissue contrast than CT (Dyson et al., 2003). The availability of standing MRI and CT is limited; therefore the major disadvantages of CT and MRI are the high cost and need for general anaesthesia (Kofler et al., 2014).

Finally, although most of the clinically relevant structures were identified in both anatomical sections and ultrasonographic, CT and MRI images, there are some potential limitations. The first is that the accuracy of an ultrasound technique is operator and machine dependent. The second is the relative small number of the MCP/MTP joints used in the CT and MRI studies; further investigations are required in clinically affected cattle. The third is the presence of dew claws, which limited the ultrasonographic examination of the palmar/plantar aspect of the MCP/MTP joint; however, CT and MRI were valuable alternatives.

The results of this study further support the use of ultrasonography for the clinical evaluation of the bovine MCP/MTP joint. The cross-sectional dimensions provided in this study may be useful for assessing tendon size alterations in cases of bilateral tendonitis or when there is minimal disruption to the internal ultrasonographic architecture of the tendon. CT and MRI provided a three-dimensional reconstruction in different planes, rendering precise visualisation and identification of the bovine MCP/MTP joint structures. The clinically relevant bony and soft tissue structures of the bovine MCP/MTP joint were identified and evaluated by CT and MRI; however, the spatial resolution of the images produced by CT did not surpass the high definition of contrast between tissues generated by MRI.

Conclusions

This study has shown that ultrasonography, CT and MRI are useful techniques for identification and description of the normal bovine MCP/MTP joint structures. This information can serve as a baseline reference for evaluation of ultrasonographic, CT and MRI scans of the bovine MCP/MTP, and may be used to assist clinicians in interpretation of pathological disorders of this joint.

Conflict of interest

None of the authors of this paper has any financial or personal relationship with other people or organisations that could inappropriately influence or bias the content of the paper.

References

- Becker, M., Heun, C., Tsousis, G., Bollwein, H., 2011. Application of computed tomography for the evaluation of obstetrically relevant measurements in German Holstein-Friesian calves. *Theriogenology* 75, 1052–1056.
- Bienert, A., Stadler, P., 2006. Computed tomographic examination of the locomotor apparatus of horses—a review. *Pferdeheilkunde* 22, 218–226.
- Boehart, S., Arndt, G., Rindermann, G., Gmachl, M., Carstjan, B., 2010. Assessment of ultrasonographic morphometric measurements of digital flexor tendons and ligaments of the palmar metacarpal region in Icelandic Horses. *American Journal of Veterinary Research* 71, 1425–1431.
- Budras, K.D., Habel, R.E., Mülling, C.K.W., Greenough, P.R., Jahrmärker, G., Richter, R., Starke, D., 2011. *Bovine Anatomy: An Illustrated Text*, 2nd Edn. Schluetersche Verlagsgesellschaft GmbH & Co. KG, Hannover, Germany 184 pp.
- Chapinal, N., Passillé, A.M., Rushen, J., 2009. Weight distribution and gait in dairy cattle are affected by milking and late pregnancy. *Journal of Dairy Science* 92, 581–588.
- Cohen, Z.A., McCarthy, D.M., Kwak, S.D., Legrand, P., Fogarasi, F., Ciaccio, E.J., Ateshian, G.A., 1999. Knee cartilage topography, thickness, and contact areas from MRI: In-vitro calibration and in vivo measurements. *Osteoarthritis and Cartilage* 7, 95–109.
- Denoix, J.M., Jacot, S., Bousseau, B., Perrot, P., 1996. Ultrasonographic anatomy of the dorsal and abaxial aspects of the equine fetlock. *Equine Veterinary Journal* 28, 54–62.
- Dyce, K.M., Sack, W.O., Wensing, C.J.G., 2010. *Textbook of Veterinary Anatomy*, 4th Edn. Saunders Elsevier, St Louis, MO, USA 864 pp.
- Dyson, S., Murray, R., 2007. Magnetic resonance imaging of the equine fetlock. *Clinical Techniques in Equine Practice* 6, 62–77.
- Dyson, S., Murray, R., Schramme, M., Branch, M., 2003. Magnetic resonance imaging of the equine foot: 15 horses. *Equine Veterinary Journal* 35, 18–26.
- Ehlert, A., Ferguson, J., Gerlach, K., 2011. Magnetic resonance imaging and cross-sectional anatomy of the normal bovine tarsus. *Anatomia Histologia Embryologia* 40, 234–240.
- Genovese, R.L., Rantanen, N.W., Hauser, M.L., Simpson, B.S., 1986. Diagnostic ultrasonography of equine limbs. *Veterinary Clinics of North America: Equine Practice* 2, 145–226.
- Gonçalves, P.V.R., Silva, L.A.F., Silva, L.H., Costa, A.P.A., Bragato, N., Cardoso, J.R., Kofler, J., Borges, N.C., 2014. Ultrasonography of the distal limbs in Nelore and Girolando calves 8 to 12 months of age. *BioMed Central Veterinary Research* 10, 102–108.
- Hagag, U., Tawfik, M., Brehm, W., Gerlach, K., 2016. Computed tomography of the normal bovine tarsus. *Anatomia Histologia Embryologia* 45, 469–478.
- Heppelmann, M., Rehage, J., Kofler, J., Starke, A., 2009. Ultrasonographic diagnosis of septic arthritis of the distal interphalangeal joint in cattle. *The Veterinary Journal* 179, 407–416.
- Kofler, J., 1996. Ultrasonographic imaging of pathology of the digital flexor tendon sheath in cattle. *Veterinary Record* 139, 36–41.

- Kofler, J., 2006. Diagnostic ultrasonography in animals—Continuation of the clinical examination. *The Veterinary Journal* 171, 393–395.
- Kofler, J., Edinger, H.K., 1995. Diagnostic ultrasound imaging of soft tissues in the bovine distal limb. *Veterinary Radiology and Ultrasound* 36, 246–252.
- Kofler, J., Geissbühler, U., Steiner, A., 2014. Diagnostic imaging in bovine orthopedics. *Veterinary Clinics of North America: Food Animal Practice* 30, 11–53.
- Kraft, S.L., Gavin, P., 2001. Physical principles and technical considerations for equine computed tomography and magnetic resonance imaging. *Veterinary Clinics of North America: Equine Practice* 17, 115–130.
- Latorre, R., Rodríguez, M.J., 2007. In search of clinical truths: Equine and comparative studies of anatomy. *Equine Veterinary Journal* 39, 263–268.
- Lee, K.J., Kishimoto, M., Shimizu, J., Kobayashi, Y., Matsumoto, K., Sasaki, N., Ishii, M., Inokuma, H., Iwasaki, T., Miyake, Y., Yamada, K., 2011. Use of contrast-enhanced CT in the diagnosis of abscesses in cattle. *Journal of Veterinary Medical Science* 73, 113–115.
- Lubbers, B.V., Apley, M.D., Coetzee, J.F., Mosier, D.A., Biller, D.S., Mason, D.E., Henao-Guerrero, P.N., 2007. Use of computed tomography to evaluate pathologic changes in the lungs of calves with experimentally induced respiratory tract disease. *American Journal of Veterinary Research* 68, 1259–1264.
- Meier, C., 1997. Vorgehensweise bei eitriger gelenksentzündung des erwachsenen rindes und klinische erfahrungen mit der spülbehandlung. *Praktischer Tierarzt* 78, 893–906.
- Nuss, K., Schnetzler, C., Hagen, R., Schwarz, A., Kircher, P., 2011. Klinische anwendung der computertomographie beim rind. *Tierärztliche Praxis Ausgabe G. Großtiere/ Nutztiere* 39, 317–324.
- O'Brien, T., Baker, T.A., Brounts, S.H., Sample, S.J., Markel, M.D., Scollay, M.C., Marquis, P., Muir, P., 2011. Detection of articular pathology of the distal aspect of the third metacarpal bone in Thoroughbred racehorses: Comparison of radiography, computed tomography and magnetic resonance imaging. *Veterinary Surgery* 40, 942–951.
- Pickersgill, C.H., Marr, C.M., Reid, S.W., 2001. Repeatability of diagnostic ultrasonography in the assessment of the equine superficial digital flexor tendon. *Equine Veterinary Journal* 33, 33–37.
- Raji, A.R., Sardari, K., Mirmahmoob, P., 2009. Magnetic resonance imaging of the normal bovine digit. *Veterinary Research Communications* 33, 515–520.
- Raji, A.R., Sardari, K., Mohammadi, H.R., 2008. Normal cross-sectional anatomy of the bovine digit: Comparison of computed tomography and limb anatomy. *Anatomia Histologia Embryologia* 37, 188–191.
- Relave, F., Meulyzer, M., Alexander, K., Beauchamp, G., Marcoux, M., 2009. Comparison of radiography and ultrasonography to detect osteochondrosis lesions in the tarsocrural joint: A prospective study. *Equine Veterinary Journal* 41, 34–40.
- Rohde, C., Anderson, D.E., Desrochers, A., St-Jean, G., Hull, B.L., Rings, D.M., 2000. Synovial fluid analysis in cattle: A review of 130 cases. *Veterinary Surgery* 29, 341–346.
- Seignour, M., Coudry, V., Norris, R., Denoix, J.-M., 2012. Ultrasonographic examination of the palmar/plantar aspect of the fetlock in the horse: Technique and normal images. *Equine Veterinary Education* 24, 19–29.
- Smith, M.A., Dyson, S.J., Murray, R.C., 2011. The appearance of the equine metacarpophalangeal region on high-field vs standing low-field magnetic resonance imaging. *Veterinary Radiology and Ultrasound* 52, 61–70.
- Smith, R.K.W., Jones, R., Webbon, P.M., 1994. The cross-sectional areas of normal equine digital flexor tendons determined ultrasonographically. *Equine Veterinary Journal* 26, 460–465.
- Solano, L., Barkema, H.W., Pajor, E.A., Mason, S., LeBlanc, S.J., Zaffino Heyerhoff, J.C., Nash, C.G., Haley, D.B., Vasseur, E., Pellerin, D., et al., 2015. Prevalence of lameness and associated risk factors in Canadian Holstein-Friesian cows housed in free stall barns. *Journal of Dairy Science* 98, 6978–6991.
- Sprecher, D.J., Hostetler, D.E., Kaneene, J.B., 1997. Lameness scoring systems that use posture and gait to predict dairy cattle reproductive performance. *Theriogenology* 47, 1179–1187.
- Starke, A., Heppelmann, M., Beyerbach, M., Rehage, J., 2007. Septic arthritis of the distal interphalangeal joint in cattle: Comparison of digital amputation and joint resection by solar approach. *Veterinary Surgery* 36, 350–359.
- Starke, A., Kehler, W., Rehage, J., 2006. Arthrotomy and arthrodesis in the treatment of complicated arthritis of the fetlock joint in adult cattle. *Veterinary Record* 159, 772–777.
- Tsuka, T., Yamamoto, N., Saneshige, M., Morita, T., Sunden, Y., Murahata, Y., Azuma, K., Osaki, T., Ito, N., Okamoto, Y., et al., 2015. Computed tomographic images of discospondylitis in a calf. *Journal of Veterinary Medical Science* 77, 1689–1691.
- Tucker, R.L., Sande, R.D., 2001. Computed tomography and magnetic resonance imaging in equine musculoskeletal conditions. *Veterinary Clinics of North America: Equine Practice* 17, 145–157.
- Van Biervliet, J., Perkins, G.A., Woodie, B., Pelligrini-Massini, A., Divers, T.J., De Lahunta, A., 2004. Clinical signs, computed tomographic imaging, and management of chronic otitis media/interna in dairy calves. *Journal of Veterinary Internal Medicine* 18, 907–910.
- Vanderperren, K., Ghaye, B., Snaps, F.R., Saunders, J.H., 2008. Evaluation of computed tomographic anatomy of the equine metacarpophalangeal joint. *American Journal of Veterinary Research* 69, 631–638.
- Vanderperren, K., Gielen, I., Van Caelenberg, A., Van der Vekens, E., Raes, E.V., Hauspie, S., van Bree, H., Saunders, J.H., 2012. Ultrasonographic appearance of bony abnormalities at the dorsal aspect of the fetlock joint in geriatric cadaver horses. *The Veterinary Journal* 193, 129–134.
- Young, B.D., Samii, V.F., Mattoon, J.S., Weisbrode, S.E., Bertone, A.L., 2007. Subchondral bone density and cartilage degeneration patterns in osteoarthritic metacarpal condyles of horses. *American Journal of Veterinary Research* 68, 841–849.